Hindawi
International Journal of Energy Research
Volume 2024, Article ID 4614066, 20 pages
https://doi.org/10.1155/2024/4614066

WILEY | Hindawi

Research Article

Thermoeconomic Analysis of a Solar-Assisted Industrial Process Heating System

Laveet Kumar,[1] **M. Hasanuzzaman**,[2] **N. A. Rahim**,[2] **and Ahmad K. Sleiti**[1]

[1]*Department of Mechanical & Industrial Engineering, College of Engineering, Qatar University, Doha, Qatar*
[2]*Higher Institution Centre of Excellence (HICoE), UM Power Energy Dedicated Advanced Centre (UMPEDAC), Level 4, Wisma R&D UM, Jalan Pantai Baharu, 59990 Kuala Lumpur, Malaysia*

Correspondence should be addressed to Laveet Kumar; laveet.kumar@qu.edu.qa

Received 25 November 2023; Revised 11 January 2024; Accepted 5 March 2024; Published 18 March 2024

Academic Editor: Muhammad Mahmood Ali

 The publication of this article was funded by Qatar National Library.

Thermal energy in the industrial sector for process heating applications in the range of 50 to 250°C consumes about 35% of the global fossil fuel. Cascaded solar thermal systems are promising solutions to meet clean and uninterrupted thermal energy supply for industrial process heating. Well-engineered cascaded arrangement of solar thermal collector (STC) and photovoltaic thermal (PVT) collector can attain an average solar fraction of more than 50%. In the present research, a solar-assisted process heating system, wherein a STC integrated in series with PVT, has been designed to produce low- to medium-temperature heat at higher solar fractions. Herein, thermal performance and economic viability of this novel system have been investigated and analyzed methodically. In the present research, a comprehensive TRNSYS simulation model is developed and validated experimentally. Results show that PVT integrated with heat pipe evacuated tube collector (PVT-HPETC) and PVT integrated with flat plate collector (PVT-FPC) system can generate thermal energy as high as 1625 and 1420 W with a thermal efficiency of 81 and 77% and exergy efficiency of 13.22 and 12.72%. Levelized cost of heat (LCOH) for PVT-HPETC at process heat temperatures of 60, 70, and 80°C is 0.214, 0.208, and 0.201 MYR/kWh, respectively. It is worth to note that LCOH is less than the existing cost of heat generation which proves that these systems are economically feasible.

1. Introduction

Global energy demand is increasing day by day due to economic evolution and modernization, and the probable future gap between energy demand and supply is projected as huge [1, 2]. Not only the industrial sector but also modern agriculture is growingly adopting various modern technologies that are transforming this sector into energy intensive [3]. To attain a global security between energy demands and supply and ensure environmental safety as well, scientists are currently emphasizing on realizing a balance between conventional fossil fuels and renewables [1]. Most of the forecasts predict that global energy consumption will increase by 33% between 2010 and 2030, the lion's share of which will be fed in the industrial sector [4]. Currently, global average industrial energy consumption is approximately 35%, which is swelling rapidly due to rapid economic growth of China, India, and other Southeast Asian countries [5]. But, the major concern with widespread and substantial burning of fossil fuels consists in the environmentally harmful CO_2 emission that alone contributes to 76% of the global warming [6].

Major industries including food processing, dyeing, drying, pulp and paper processing, and petroleum refining utilize fossil fuels to produce process heat in the form of either steam or boiling water [7, 8]. Globally, industrial sector generates about a cumulative 47% of the emissions through burning fossil fuels [9]. Hence, increasing the span of renewable energy application in process industries and reducing fossil fuel consumption must be traded off in order to alleviate industrial emissions [10]. Environmental issues with the fossil fuels together with their fast depletion are putting an urgency to adopt renewables as an alternative, in which solar energy comes in the first place since it is

practically inexhaustible and accessible in direct and indirect forms [11, 12]. World leaders have agreed to encounter approximately 45% of the global energy demand with solar energy by 2050 [13].

Energy from the sun can be harvested in the form of heat and electricity, wherein conversion efficiency of solar to thermal is essentially superior [14, 15]. Furthermore, conversion efficiency of solar thermal collectors (STC) is better than the conventional electric heaters [16–18]. In this regard, photovoltaic thermal (PVT) systems can be envisaged as another option since they deliver dual output—heat and electricity. However, a downside of PVT technology is that it can produce only low-temperature thermal energy in the range of 35 to 40°C [12, 19]. A vast potential implementation of solar thermal in industrial process heat (IPH) is still in its budding phase since commercial application needs heat generation at the medium- to high-temperature range [20]. To upraise the application of solar thermal in IPH, a novel concept of an integrated solar-assisted process heating system composed of PVT with STC can serve to overcome the drawbacks of the isolated systems.

In the literature, research related to energetic and exergetic analysis of the individual PVT and FPC has been reported by numerous researchers. The energy and exergy analysis of glazed and unglazed PVT system has been investigated by Kazemian et al. [21–23], reporting that thermal energy and exergy efficiency of glazed PVT (74.14 and 0.76%) is greater than unglazed PVT (71.29 and 0.65%); however, it is opposite for electrical energy and exergy efficiency, i.e., it is greater for unglazed PVT (14.17 and 13.47%) than glazed PVT (13.40 and 12.99%), respectively. Similar works by various researchers [24–27] have reported that thermal efficiency of glazed PVT is more than unglazed PVT, while the trend is reversed for electrical efficiency. In addition, the effect of various designs of thermal absorbers in PVT has demonstrated a remarkable effect of increase in thermal and electrical performance as investigated by [28–33]. However, the major drawback of the PVT system is that it cannot give high thermal output, and if arrangements are made to achieve higher thermal output, it will greatly increase the cell temperature, and ultimately, it decreases the electrical efficiency.

Compared to the PVT system, the FPC system can output high-grade thermal energy and higher outlet temperature having drawback as zero electricity generation. The energy and exergy analysis of FPC has been investigated by Tong et al. [34] reporting the energy and exergy efficiency (63.6 and 1.25%) for water as a working fluid; however, adding the nanoparticles in the water in the flat plate solar collector could improve the energy and exergy efficiency. In addition, similar results from the previous studies of FPC [35–42] reported that the energy and exergy efficiency of solar collector ranged from 40 to 71% and 2 to 8.78%, respectively, and varies depending upon the design of FPC, operating parameters, and type of working fluid. Also, [43, 44] carried out the energy and exergy analysis for FPC with phase change material (PCM) and reported the average energy and exergy efficiencies in the range of 40 to 45% and 2 to 3.5%, respectively.

Recently, for the first time, a steady two-dimensional mathematical model has been modeled for the integrated system for both PVT and STC, and this model is validated from other articles and previous work [19, 45]. Although a good number of simulation and experimental studies on isolated systems have been reported in literature, but detailed workable simulation model for integrated system and its real-time experimental validation is yet to be carried out. Also, no transient system simulation is available to perform parametric analysis of various parameters of an integrated system including water inlet temperature, mass flow rate, outlet temperature, ambient temperature, solar thermal collector heat gain, and rate of heat supplied from auxiliary system. Moreover, the long-term performance of such SAPH systems is yet to be analyzed extensively. In the present research, dynamic simulation models of two novel solar-assisted cascaded systems (PVT-FPC and PVT-HPETC) have been designed and developed together with three isolated systems (PVT, FPC, and HPETC). The well-engineered cascaded system can supply uninterrupted industrial process heat as per required industrial temperature ranges. All the systems have been modeled and simulated in TRNSYS, and outdoor experimental analysis has been carried out under typical Malaysian conditions to validate the models. This research is aimed at presenting a comparative analysis of the cascaded system over against three isolated systems, viz., PVT, FPC, and HPETC based on energy, exergy, and economic analysis to examine the aptness of the novel cascaded systems.

2. Methodology

The methodical phases in resolving the research problem have been discoursed in detail in this research. A combination of simulation and on-site experimental investigation has been adopted in this research work. To limit experimental uncertainties, apposite assumptions made during simulation are examined meticulously. A solar-assisted process heating (SAPH) system is an isolated solar thermal collector (be it an FPC or HPETC) or multiple collectors cascaded in series or solar thermal collector integrated with photovoltaic thermal (PVT) collector producing an outlet temperature to serve industrial process heating (IPH) purpose. The concept of a SAPH system comprised of PVT and STC. The PVT collector converts a portion of the incident solar radiation into electricity, the remaining energy being dissipated as heat is utilized to preheat the heat transfer fluid (HTF: water). Afterwards, the preheated water passes through the STC, which further heats up the water and raises the outlet temperature to a desired level. The water outlet temperature can be regulated by adding more collectors in series and also by controlling the HTF flow rate to some extent. This high-temperature water can be directly employed for IPH applications or stored as sensible or latent heat storage and supplied to application ends. In the meantime, the electricity produced from PVT is used to run a DC electric water heater to supply auxiliary heat that can ensure an uninterrupted supply of heat.

2.1. Model Development. Cascaded SAPH consists of a solar thermal collector (either FPC or HPETC) connected in

series with a PVT collector. The setting is such that the outlet water of PVT flows into the FPC or HPETC, which further gets heated by the solar irradiance. Based on this idea, a detailed cascaded SAPH model is built in TRNSYS for performance evaluation in this section. Figure 1 displays the block diagram of a TRNSYS model. The different components used throughout in the configuration of the TRNSYS model as seen in the block diagram are as follows. (1) Type 109 is a weather data reader. (2) Type 50a is a PVT collector which transforms the solar irradiance into electrical and thermal energy. (3) Type 1b and 71 are a flat plate collector (FPC) and a heat pipe evacuated tube collector (HPETC) that also transforms the solar irradiance into the thermal energy. (4) Type 3b is a water pump. (5) Type 6 is an electric heater that provides additional auxiliary heat to the working fluid for the desired outlet temperature. (6) Type 65d and 25c are on-line plotter and printer.

2.2. Experimental Investigation. In solar research, outdoor studies are preferable since they can authentically portray the real-time performance of any system. Therefore, the present experimental investigation has been carried out in the Solar Garden of UM Power Energy Dedicated Advanced Centre (UMPEDAC), University of Malaya, Kuala Lumpur, Malaysia. This outdoor solar research establishment is situated at 3.1169°N and 101.6669°E. The average ambient temperature of the experimental site is 27.63°C, varying between the limits of 32.67°C and 24.24°C, respectively. Annual rainfall is between 1800 to 3900 mm, average humidity is about 80%, and wind speed is 1.79 m/s in December and 2.10 m/s in January. Maximum daily global solar irradiance and direct normal irradiance are 1068 W/m^2 and 915 W/m^2, respectively [46].

The integrated solar-assisted process heating (SAPH) system comprises of a PVT module and an FPC and HPETC connected in series. The schematic and experimental setup of SAPH as shown in Figures 2(a) and 2(b) has an FPC and HPETC integrated with a PVT collector and an auxiliary DC electric water heater with forced circulation by means of a pump and closed distribution to storage tanks. The measurement ranges and accuracy of the instruments used are given in Table 1.

After the modeling and simulation have been completed, all systems were mounted on metallic structures held at an angle of optimum magnitude (calculated using equations (1) and (2)) facing to the south in order to intercept the maximum radiations throughout the day. Cooper's equation as employed for slope calculation is given by [33, 47]

$$\delta = 23.45 \ \sin\left[\frac{(284 + n_1)}{365} \times 2\pi\right], \tag{1}$$

$$\beta = (Q_1 - \delta), \tag{2}$$

where δ is the solar declination, n_1 is the day of the year, and β is the angle of inclination. In equation (1), the term 23.45 is in degrees, and the term within the parenthesis is in radian.

2.3. Mathematical Framework

2.3.1. Energetic and Exergetic Analysis. The basic principle of energy analysis is based on the first law of thermodynamics that consists of energy balances and evaluating the energy efficiencies. The equations are given as [45, 48, 49]

$$\begin{aligned}
&\sum \dot{E}_i = \sum \dot{E}_o + \sum \dot{E}_{\text{loss}},\\
\text{or}\quad &\dot{E}_s + \dot{E}_{m,i} = \dot{E}_{m,o} + \dot{E}_{\text{el}} + \dot{E}_{\text{loss}},\\
&\dot{E}_{s(\text{CS})} = \dot{E}_{s(\text{PVT})} + \dot{E}_{s(\text{FPC or HPETC})},\\
&\dot{E}_{s(\text{PVT})} = \tau\alpha A_{\text{PVT}} I,\\
&\dot{E}_{s(\text{FPC})} = \tau\alpha A_{\text{FPC}} I \quad \text{or} \quad \dot{E}_{s(\text{HPETC})} = \tau_{\text{gco}}\tau_{\text{gco}}\alpha_c A_{\text{HPETC}} N_{\text{hp}} I,
\end{aligned} \tag{3}$$

Heat gain:

$$\begin{aligned}
\dot{E}_{g(\text{CS})} &= \dot{E}_{m,o(\text{FPC or HPETC})} + \dot{E}_{m,i\,(\text{PVT})}\\
&= \dot{m}C_p\left(T_{o(\text{FPC or HPETC})} - T_{i(\text{PVT})}\right),
\end{aligned} \tag{4}$$

Thermal (energy) efficiency:

$$\begin{aligned}
\eta_{\text{Thermal}(CS)} &= \frac{\dot{E}_g}{\dot{E}_{s(\text{PVT})} + \dot{E}_{s(\text{FPC or HPETC})}}\\
&= \frac{\dot{m}C_p(T_o - T_i)}{\tau\alpha A_{\text{PVT}} I + \tau\alpha A_{(\text{FPC or HPETC})} I}.
\end{aligned} \tag{5}$$

Exergy is the amount of energy that would transform to productive use. The basic principle of exergy analysis is defined on the basis of the second law of thermodynamics, which states that the thermal energy cannot be transformed without the change of temperature. Equations for thermal and electrical exergy equations are given as [49–52]

$$\begin{aligned}
&\sum \dot{E}_{x_i} = \sum \dot{E}_{x_o} + \sum \dot{E}_{x_{\text{dest}}},\\
\text{or}\quad &\dot{E}_{x_s} + \dot{E}_{x_{m,\text{in}}} = \dot{E}_{x_{m,o}} + \dot{E}_{x_{\text{el}}} + \dot{E}_{x_{\text{dest}}},\\
&\dot{E}_{x_{s\,(\text{CS})}} = \dot{E}_{x_{s\,(\text{PVT})}} + \dot{E}_{x_{s\,(\text{FPC or HPETC})}},\\
&\dot{E}_{x_{s\,(\text{PVT})}} = A_{\text{PVT}} I_{\text{rad}}\left(1 - \frac{T_a}{T_s}\right),\\
&\dot{E}_{x_{s(\text{FPC or HPETC})}} = A_{\text{FPC/HPETC}} I_{\text{rad}}\left(1 - \frac{T_a}{T_s}\right),
\end{aligned} \tag{6}$$

where T_s is sun temperature which is considered as 5,777 K.

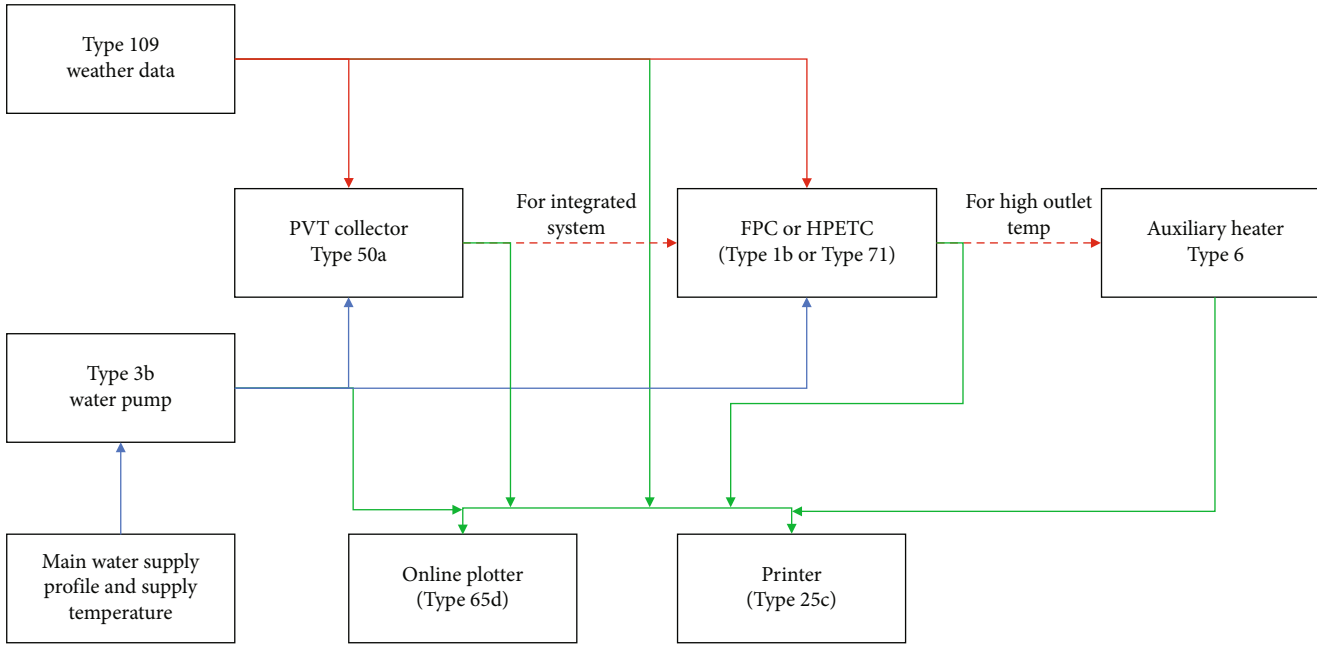

Figure 1: TRNSYS model block diagram.

Thermal exergy efficiency:

$$\varepsilon_{\text{th(CS)}} = \frac{\dot{E}_{x_{\text{th}}}}{\dot{E}_{x_{s(\text{PVT})}} + \dot{E}_{x_{s(\text{FPC or HPETC})}}} = \frac{\dot{m}\, C_p \left[\left(T_{o(\text{FPC or HPETC})} - T_{i(\text{PVT})}\right) - T_a \ln\left(T_{o(\text{FPC or HPETC})}/T_{i(\text{PVT})}\right)\right]}{A_{\text{PVT}}\, I_{\text{rad}}\,(1-(T_a/T_s)) + A_{(\text{FPC or HPETC})} I_{\text{rad}}(1-(T_a/T_s))}. \tag{7}$$

Electrical exergy efficiency:

$$\varepsilon_{\text{el(CS)}} = \frac{\dot{E}_{x_{\text{el}}}}{\dot{E}_{x_{s(\text{PVT})}}}. \tag{8}$$

Overall exergy efficiency:

$$\varepsilon_{\text{ov(CS)}} = \frac{\dot{E}_{x_{\text{th}}}}{\dot{E}_{x_{s(\text{PVT})}} + \dot{E}_{x_{s(\text{FPC or HPETC})}}} + \frac{\dot{E}_{x_{\text{el}}}}{\dot{E}_{x_{s(\text{PVT})}}}. \tag{9}$$

2.3.2. Uncertainty Analysis. An uncertainty analysis is performed on both thermal and electrical parameters for both energy and exergy analysis. Suppose that parameters $u_1, u_2, u_3, ..u_m, u_{m+1} \cdots .u_n$ are measured with uncertainties $\delta u_1, \delta u_2, \delta u_3, .., \delta u_m, \delta u_{m+1}, \cdots \delta u_n$, then the fractional uncertainty of U is written as [53]

$$\frac{\delta U}{U} = \sqrt{\left(\frac{\delta u_1}{u_1}\right)^2 + \left(\frac{\delta u_2}{u_2}\right)^2 + \left(\frac{\delta v_2}{u_3}\right)^2 + \cdots \left(\frac{\delta u_m}{u_m}\right)^2 + \left(-\frac{\delta u_{m+1}}{u_{m+1}}\right)^2 + \left(-\frac{\delta u_n}{u_n}\right)^2}. \tag{10}$$

Using the above equation (10) and equations of energy and exergy efficiency, fractional uncertainties can be calculated. The uncertainties of the measuring instruments are given in Table 1. Employing the above analysis, the maximum uncertainty is calculated and found to be less than 5.0% for all parameters. Therefore, uncertainty values within this limit indicate the reliability of the measured data [53].

2.3.3. Economic Analysis. In the present research, the discounted cash flow (DCF) method has been adopted that employs three criteria, viz., NPV, IRR, and PBP in selecting the most economical and profitable project [11, 54]. The economic analysis is conducted based on the thermal performance of isolated and cascaded systems. Table 2 presents the main assumptions and parameters which have been used in the present economic analysis.

(1) Net Present Value (NPV). NPV is expressed by [11]

$$\text{NPV} = -C_0 + \sum_{i=1}^{N} \frac{C_i}{(1+r)^i}, \tag{11}$$

where NPV is the net present value index, C_0 is the initial investment cost, C_i is the expected cash flow in the i-th period (i-th month or year), r is the discount rate, and i is the number of project plant life periods (months or years). The expected cash flow consists of all incomes and expenditures of the project during the plant life. In this method of evaluation, if the NPV of a project is positive, the project is considered acceptable, economical, and profitable. While if the NPV is negative, it will be evaluated as unacceptable and nonprofitable.

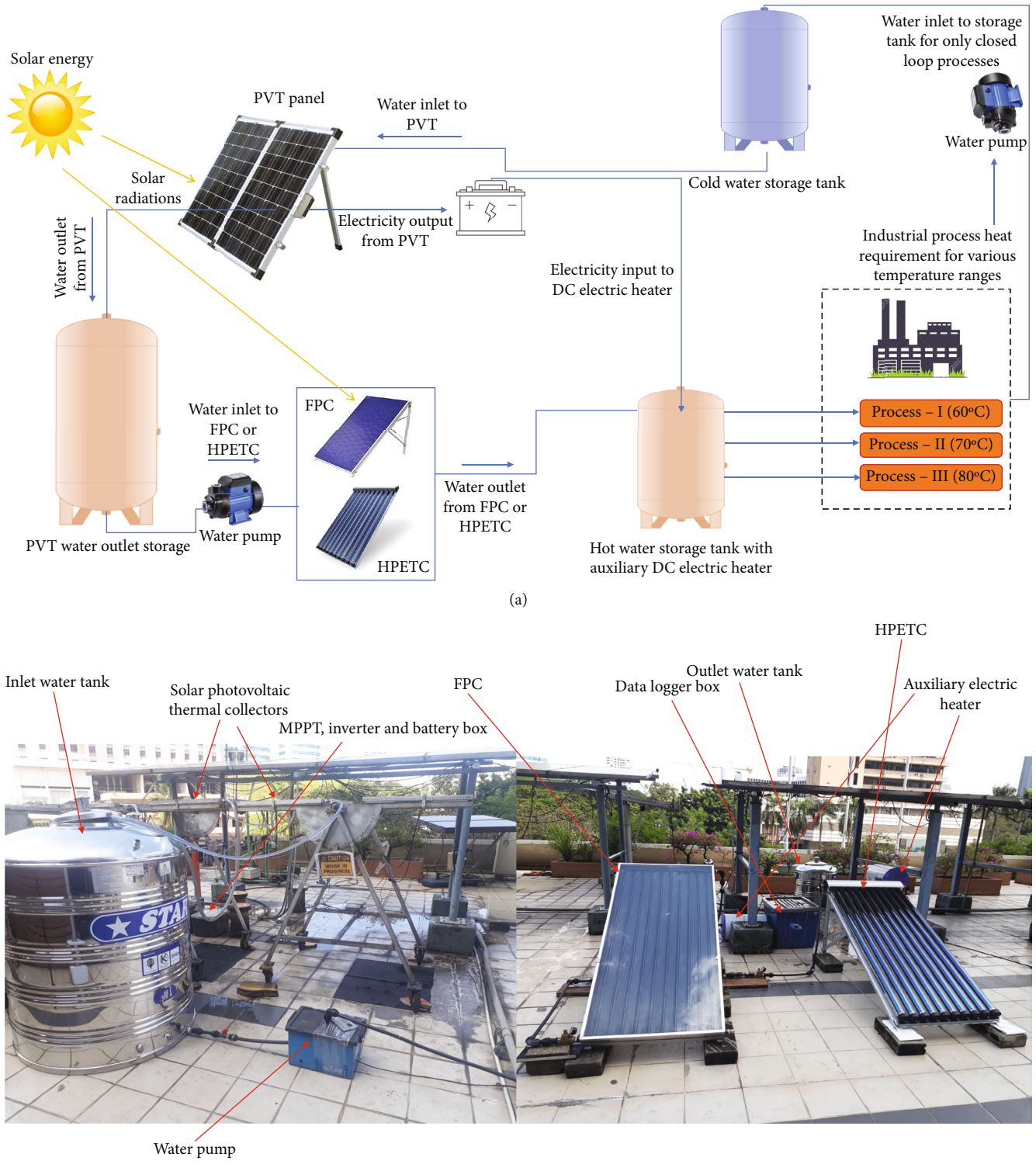

Figure 2: (a) Schematic and (b) experimental setup of the SAPH system.

(2) Internal Rate of Return (IRR). IRR is obtained from the NPV formula considering a zero net present value [11].

$$\text{NPV} = 0 \Rightarrow \text{NPV} = -C_0 + \sum_{i=1}^{N} \frac{C_i}{(1+\text{IRR})^i}. \quad (12)$$

Based on this method of assessment, if the project rate of return is more than the interest rate of investment, then the project is considered economical; if it is less, then the plan will be evaluated nonprofitable. The net income of successive years is discounted to year zero at the rate that comply with the minimum attractive rate of return (MARR). Once the

Table 1: Measurement ranges and accuracy of the instruments and sensors.

Instrument	Measuring range	Accuracy
Data logger (model: DataTaker DT80)	-270 to 1372°C	±2%
Pyranometer (model: LI-COR, LI200R)	0 to 2000 W/m^2	±5%
Digital flow meter (model: Gardena, 8188-20)	0.5 to 30 LPM	±0.5
Thermocouple (K-type)	-200 to 1000°C	±5%

Table 2: Parameters and assumptions for economic analysis.

Input parameters	System		
	PVT	FPC	HPETC
Total capital cost with DC water heater (RM per m^2)	2714	2613	2814
Total operation and maintenance costs (RM per m^2)	150	125	150
Interest rate (%)		14	
Discount rate (%)		8	
Incremental cost/year (%)		3	
Electricity price (RM/kWh) (TNB tariff)		0.365	
Plant life period (year)		20	
Other revenue income		CERs from CDM: Global high scenario (80 USD per ton) Global low scenario (40 USD per ton)	
Degradation rate		5%	

Note: 1 USD is taken as 4.27 MYR during the conduct of this research study.

IRR is calculated, it should be compared with the MARR. If the IRR is greater than MARR, the investment is economically viable. If the IRR is lower than MARR, the investment is not economically interesting. When IRR and MARR are equal, the investor is economically indifferent between the project and the opportunity cost. Similar to the NPV, the project with the highest IRR is also financially more interesting [55].

(3) Payback Period (PBP). Equations (13) and (14) are used to calculate the PBP. The value of n, which is obtained from the equations, shows the period that the total initial investment of the project returns to the investors. So, a project which has less n index is more economical and more attractive to investors [11].

$$-C_0 + \sum_{i=1}^{N} (\mathrm{CF})_i = 0, \tag{13}$$

$$n = \frac{C_o}{\mathrm{CF}}. \tag{14}$$

where C_o is the cash flow of i-th period and CF is the equivalent annual cash flow.

(4) Levelized Cost of Heat (LCOH). In order to compare differing system designs, a standard metric named levelized cost of energy is employed that combines two disparate energy flows into one bottom-line metric. The levelized cost of heat (LCOH), adopted in the present analysis, allows a side-by-side comparison of differing solar thermal technologies and technical specifications which examines the technical and financial factors affecting the cost of heat production of a SAPH system. Levelized cost of heat (LCOH) is calculated by dividing the lifetime cost of the system by the lifetime energy generation. The cost of the system is calculated by summing the annual net cash flow attributed to the installation and operation of the system, including expenses and revenue, over the lifetime of the system. In order to improve (reduce) the LCOH, either the cash flow needs to be reduced by mitigating costs or the energy generation must be increased through technical advances, such as improved efficiency.

Conventional solar thermal systems collect the entire spectrum of light, and the high energy ultraviolet and visible regions of the spectrum are arguably more valuable when harvested as electricity considering the relative cost of electricity (2–3× higher than natural gas). Because of this, there have been several projects dedicated to developing hybrid systems for combined heat and power applications. Such hybrid systems can attain improved energy or exergy efficiency relative to standalone systems. The electricity produced from the PV can be used to offset the electricity usage in a facility, effectively saving on power costs. This cost savings can be added into the cash flow calculations, reducing the overall annual operation costs. In this manner, the overall LCOH can be reduced compared to conventional

solar thermal systems. Herein, a LCOH model has been presented which examines the technical and economic factors which affect the cost of heat production for a hybrid system using the electricity produced to subsidize the cost of heat.

The LCOH is calculated using equation (15). The annual cash flow (equation (16)) is comprised of the savings from electricity generation (+) based on the cost of electricity and operation and maintenance (O&M) costs (−) including both photovoltaic and thermal components. The annual present value was calculated based off a nominal discount rate (dr) of 8% using equation (17) where n is the year of operation. The net present value (NPV) for a lifetime of 20 years was calculated by summing the annual present values and subtracting the initial up-front capital cost. Yearly thermal and electrical energy generation was taken from the previous analysis. The electricity generation was used in combination with the price of electricity to calculate the electricity savings for annual cash flow. Like the cash flow, the present value of thermal energy generation was discounted at 8% annually. The NPV for thermal generation was the summation of annual present values as represented in equation (18) [56]. Only the thermal energy was included in the NPV for energy generation, as heat is what is being priced.

$$\mathrm{LCOH} = \frac{\sum_{i=1}^{N} \mathrm{PV}_{\mathrm{CF}}}{\sum_{i=1}^{N} \mathrm{PV}_{\mathrm{th}}}, \tag{15}$$

$$\mathrm{CF}_n = \mathrm{ES}_n - \mathrm{OM}_n, \tag{16}$$

$$\mathrm{PV}_{\mathrm{CF}} = \frac{\mathrm{CF}_n}{(1+\mathrm{dr})^n}, \tag{17}$$

$$\mathrm{PV}_{\mathrm{th}} = \frac{E_{\mathrm{th}}}{(1+\mathrm{dr})^n}. \tag{18}$$

3. Results and Discussion

The outcomes of the present research along with corresponding physical explanations are described in this section. Data were collected for the incessant flow of hot water at required ranges of temperature and flow rates ranging from 0.5 to 4.0 LPM and variation of solar radiation from 0 to 1000 W/m^2.

3.1. Modeling and Experimental Validation. The simulation models of the two SAPH systems modeled and simulated in TRNSYS have been validated using real-time experimental assessment. It can be seen from Figure 3 that the simulated and experimental results of water outlet temperature based on variation in solar irradiance agree quantitatively and qualitatively for both PVT-FPC and PVT-HPETC configurations. For the validation, the data is extracted from the comprehensive dataset of experimental values collected over several months. The thoroughgoing compliance of the simulation and experimental outcomes confirms the validity of the TRNSYS model in predicting the thermal and electrical behavior of the cascaded systems.

3.2. Thermal Performance Analysis

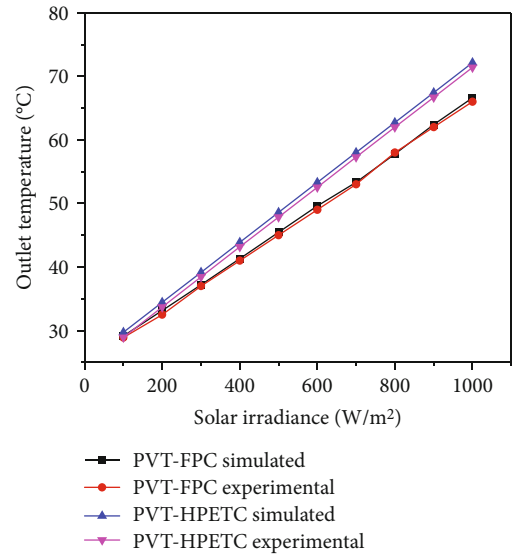

Figure 3: Comparison between simulated and experimental results of water outlet temperature.

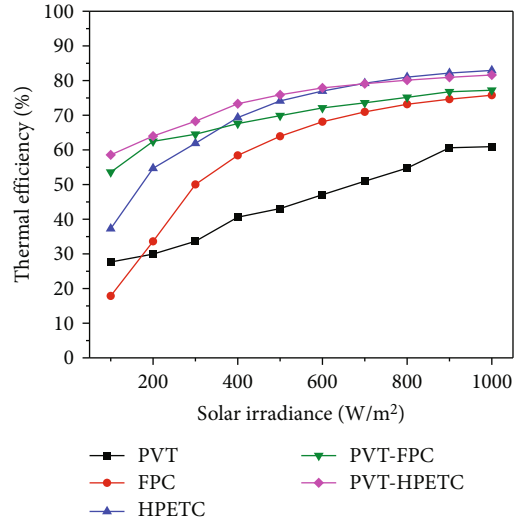

Figure 4: Effect of variation of solar irradiance on thermal efficiency.

3.2.1. Energetic Analysis. In this section, energy interactions of the cascaded SAPH and the isolated systems have been presented. Cascading PVT with FPC and HPETC not only augments thermal performance, but it aids to maintain the thermal efficiency at various flow rates. The thermal efficiency for isolated PVT, FPC, and HPETC decreases rapidly with an increase in flow rate, but as for cascaded units, the thermal efficiency is steady and stable, particularly after 1.5 L/min. This is a necessary characteristic of the cascading FPC and HPETC with PVT. The advantages of hybridization will be further shown in Figure 4, which indicates that the thermal performance of the cascaded PVT-HPETC and PVT-FPC systems is still considerably higher, well below the minimum degree of solar irradiance. From Figure 4, it

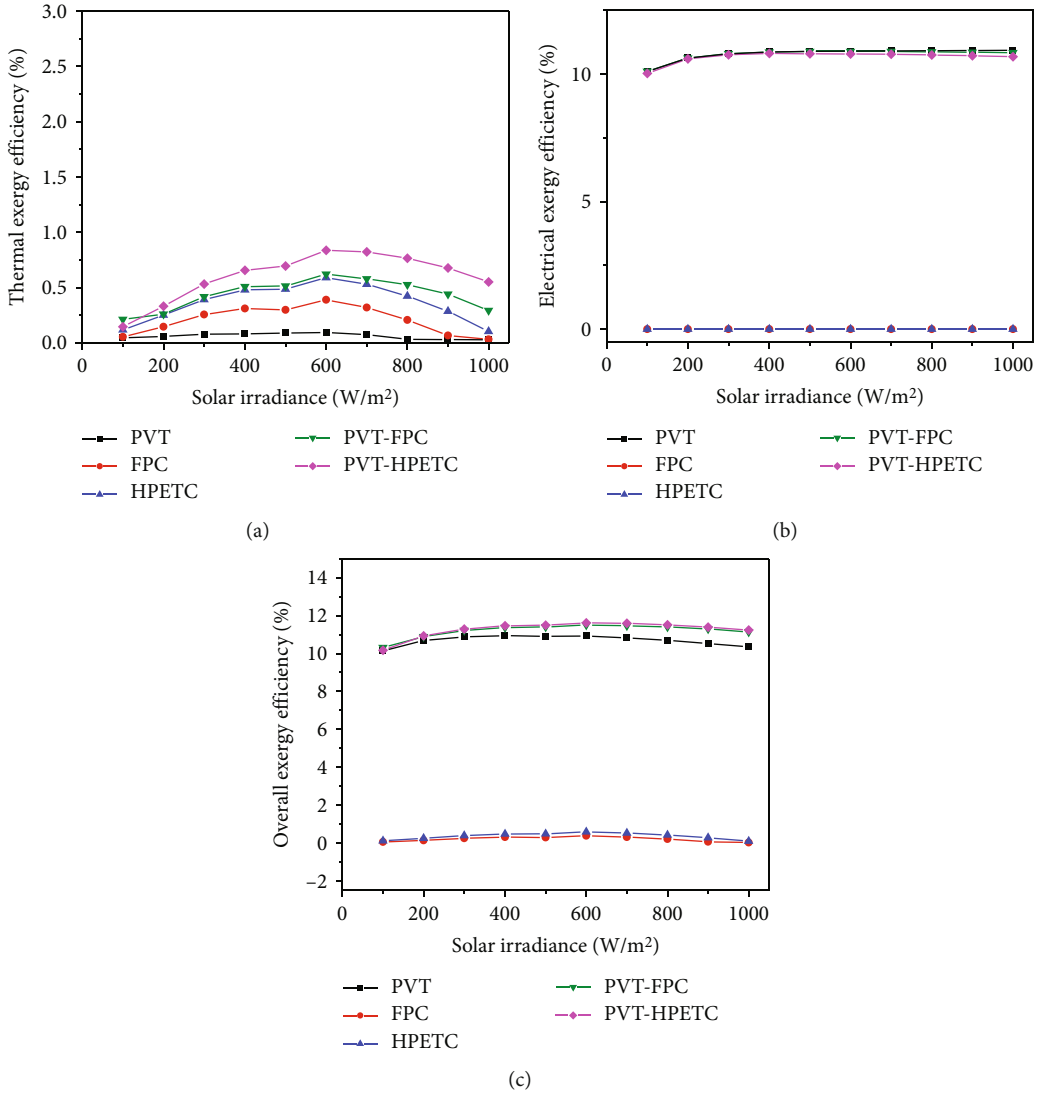

Figure 5: Effect of variation of solar irradiance on (a) thermal, (b) electrical, and (c) overall exergy efficiency.

would have been seen that the minimum thermal efficiency of cascaded PVT-HPETC and PVT-FPC systems is approximately 58.56 and 53.57%, respectively, which is obtained at very low solar irradiance of 100 W/m^2, whereas the thermal efficiency of individual HPETC and FPC system with the same degree of solar irradiance is near 37.28 and 17.86% only. From Figure 4, it can also be seen that the maximum thermal efficiency of cascaded PVT-HPETC and PVT-FPC systems is approximately 81 and 77%, respectively, which is obtained at very low solar irradiance of 1000 W/m^2. The literature work on the cascaded PVT and STC system is not available; however, in many experimental research on the PVT system, the energy efficiency ranges between 35 and 74% have been reported [14, 21, 22, 25, 30, 32, 33, 57–61]. Similarly, results for energy efficiency of FPC and HPETC systems are reported in the range of 25-71% [34–36, 38, 41, 62, 63] and 30-85% [64, 65], respectively. Ayompe et al. [66] also compared the thermal performance of FPC and HPETC and reported that the HPETC system proves its better performance compared to the FPC which is also proved in this study. Overall, among all the systems, the cascaded system has better advantages over other individual systems as it can obtain a high output temperature with high thermal heat gain and efficiency.

3.2.2. Exergetic Analysis. In this section, the actual available efficiency for isolated as well as cascaded systems has been investigated. The effects of solar irradiance on the thermal, electrical, and overall exergy efficiency have been presented in Figure 5. It can be seen that the electrical exergy parameter of PVT and PVT cascaded with FPC and HPETC units is similar and varies insignificantly under varying solar irradiance; thus, thermal exergy parameter determines the overall efficiency trend. The effect of solar irradiance on thermal exergy efficiency defines a bell-shaped curve where the thermal exergy efficiency increases to a solar irradiance of 600 W/m^2 and then ultimately decreases. The highest thermal exergy efficiency achieved by the PVT-HPETC and

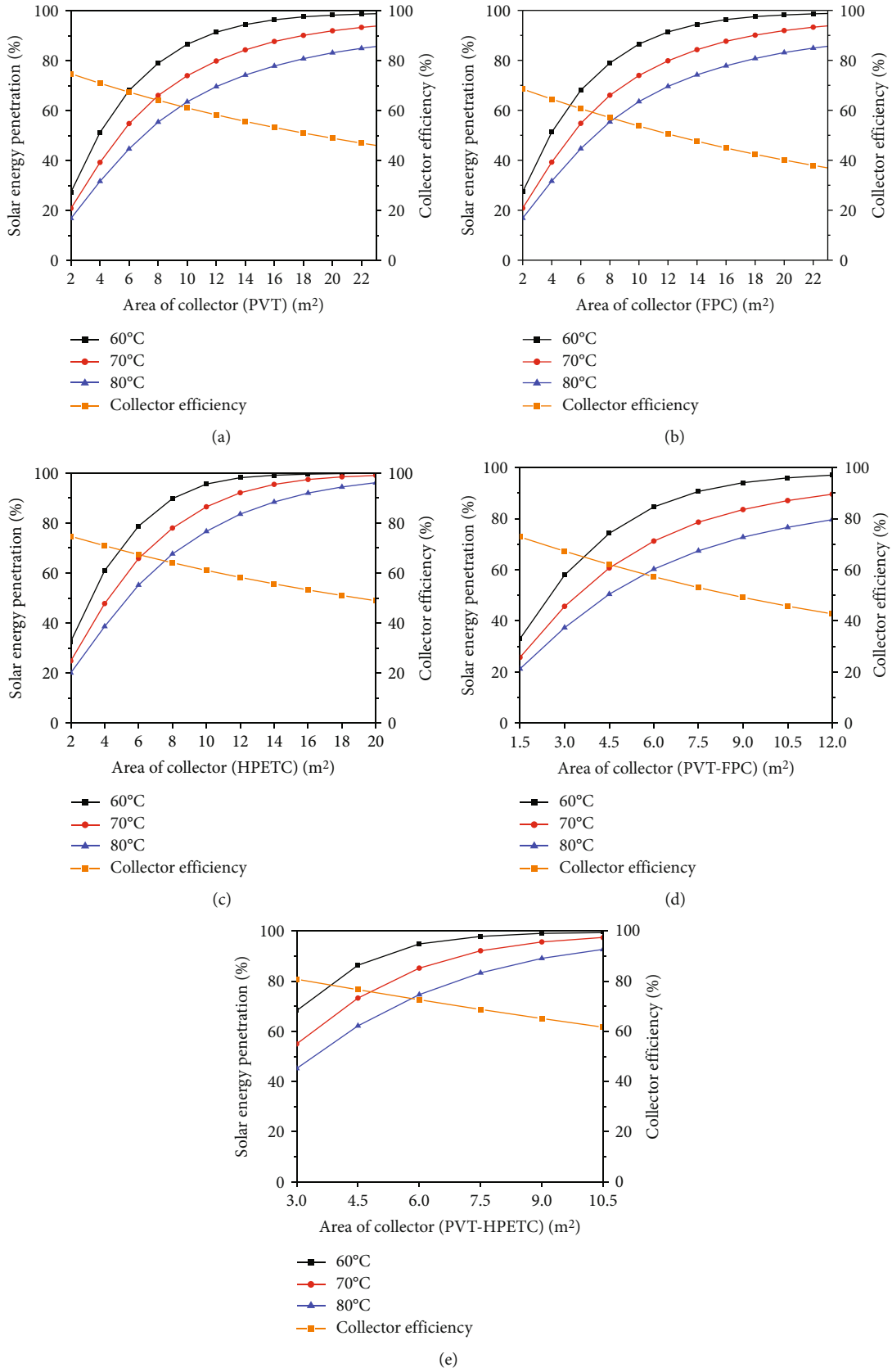

Figure 6: Optimized area: (a) PVT, (b) FPC, (c) HPETC, (d) PVT-FPC, and (e) PVT-HPETC configurations.

Table 3: Summary table for area optimization.

System	Process temperature (°C)	Solar energy penetration (%)	Optimized area (m^2)	η_{Col} (%)
PVT	60	67.50	5.92	67.41
	70	64.54	7.72	64.50
	80	61.67	9.54	61.76
FPC	60	61.79	5.26	62.10
	70	59.29	6.74	59.06
	80	56.59	8.26	56.51
HPETC	60	69.14	4.93	69.25
	70	66.68	6.21	67.01
	80	64.95	7.55	64.72
PVT-FPC	60	65.01	3.64	65.10
	70	61.58	4.62	61.63
	80	58.26	5.67	58.30
PVT-HPETC	60	78.50	3.85	78.40
	70	75.71	4.81	75.30
	80	73.10	5.81	73.06

PVT-FPC systems is significantly low at just 0.83% and 0.69% as shown in Figure 5. However, the exergy efficiency of the cascaded device is comparatively higher due to the electrical exergy addition. Figure 5 also indicates that the overall exergy efficiency of the PVT-HPETC and PVT-FPC systems is more than 11.12 and 12.72% under varying solar irradiance, respectively. Related patterns for the exergetic analysis have been found in the literature on PVT, FPC, and HPETC. It has been shown that the exergy efficiency of the PVT system varies from 11 to 14% [21, 24–26, 33, 50, 67]. However, for STC, it is very low and reported to vary between 2 and 9% [34–36, 38, 39].

3.2.3. Optimization of the Collector Configuration. The amount of solar energy harvest from a solar thermal system directly depends on the area of collector. On the other hand, there is a certain limit for solar energy availability even in the daytime; hence, in industrial process heating (IPH) applications, it is not practicable to assume solar energy penetration ("solar energy penetration" refers to contribution in the total heat requirement) more than 40-50%. Moreover, there exists an inverse relationship (though not linear) between collector efficiency and span of the collector. Hence, collector area optimization becomes an important issue in large-scale solar thermal applications. This section presents the optimization practice of solar collector area for industrial process heat requirements.

It may be noted from Figures 6(a)–6(e) that with an increase in area of the collector, the solar energy penetration for all systems increases for every process heat temperatures (60, 70, and 80°C), the rate of increment being steep up to a certain area and rather bland after that. In contrast, the collector of efficiency decreases. Therefore, it is necessary to have a trade-off between the collector efficiency and solar energy penetration for an optimum area of collector which can fulfil the minimum industrial process heat (IPH) requirements. Therefore, in this research, solar energy penetration share is obtained in the range of 50–80% due to intermittency of the renewable energy sources, and according to this range, the optimized area of solar thermal collector required is estimated. This is a significant and attractive consideration in applying these technologies to utilize solar energy. Also, summarized results for the optimized area are given in Table 3.

3.3. Economic Feasibility Analysis. From the energetic and exergetic analysis, it has been confirmed that the thermal performance of isolated HPETC and cascaded PVT-HPETC is better than other systems, while the total investment needed for FPC and PVT is lower than that of HPETC or PVT-HPETC. So, economic aspects become significant for final selection between these collectors for solar-assisted process heating in IPH to be justified for commercial installation.

Economic feasibility analyses of different SAPH systems have been presented for Malaysian weather conditions. The analysis has been carried out for three different processes temperatures such as 60, 70, and 80°C. It has already been revealed from thermal performance of the systems that these systems perform better at 1.0 LPM, so the economic analysis is primarily done for the optimized flow rate of 1.0 LPM.

As a part of economic analysis, NPV, IRR, and PBP of five different SAPH systems have been evaluated for diverse criteria like with and without CERs. CERs are additional source of revenue that are basically awarded by the United Nations (UN) to member nations for preventing one ton of carbon dioxide emissions [68]. These are usually issued to member states for projects achieving greenhouse gas reductions using Clean Development Mechanisms (CDM). CDMs make it possible for these projects to occur and set

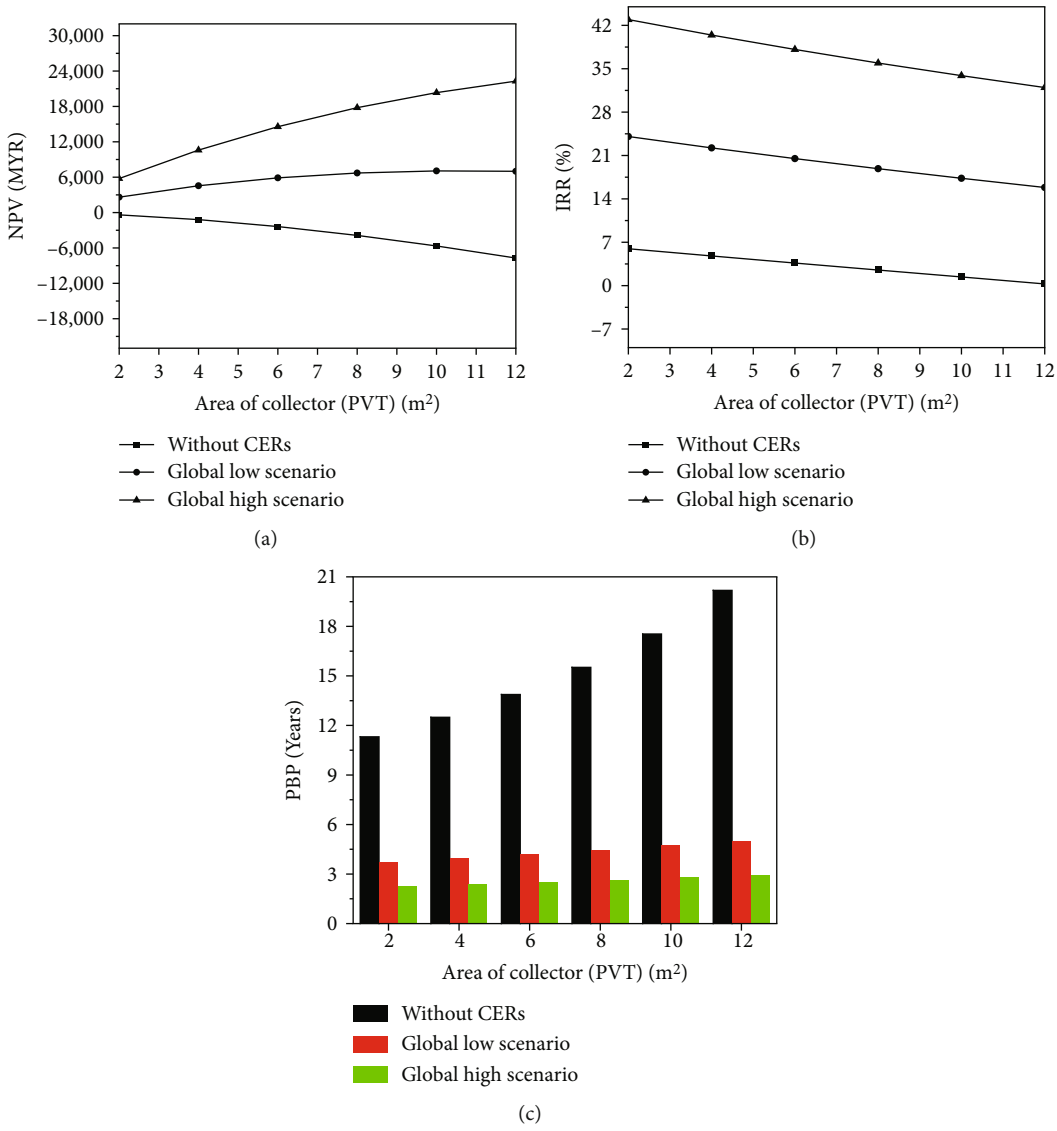

Figure 7: Variation in (a) NPV, (b) IRR, and (c) PBP as a function of collector area for isolated PVT system.

a baseline for future emission targets. It is assumed that investment is done from the owners' equity, and no part of investment is borrowed from any financing institutions in the form of bank loan or mortgage for simplicity. Gross profit is calculated by deducting the cost of industrial process heat from the revenue generated by the sale of the generated process heat. Earnings before tax (EBT) is evaluated from the revenue earning from business, and supportive additional income from the certified emission reductions (CERs) was considered as an alternative case. Similarly, earning after tax (EAT) is found after deduction of tax after ten years of plant operations, the first ten years for a renewable energy project being exempted from tax [69].

3.3.1. NPV, IRR, and PBP Analysis. Net present value (NPV), internal rate of return (IRR), and payback period (PBP) have been evaluated based on different criteria, namely, with and without certified emission reductions (CERs). Two subscenarios, viz., global high scenario (GHS) and global low scenario (GLS) in the case of CER have been considered in accordance with World Bank Report 2019 [70].

In evaluating NPV, IRR, and PBP for the isolated and cascaded SAPH systems, several prolepsis and parameters have been assumed (Table 2). Carbon emissions price per ton in the case of GHS and GLS are taken as US$ 80 and US$ 40 per ton, respectively. NPV, IRR, and PBP are calculated from equations (11)–(14) for all five systems in accordance with energetic and exergetic viewpoints. In NPV, the total future revenues are converted into the equivalent earnings at the beginning time of the project, and then, the required initial capital of project is deducted from it. For the IRR, a discount rate is calculated from the discounted income of project to the amount of investment. IRR is the rate of return which equals the present value of project income to the present value of its costs that makes the NPV of all cash flows from a particular project equal to zero.

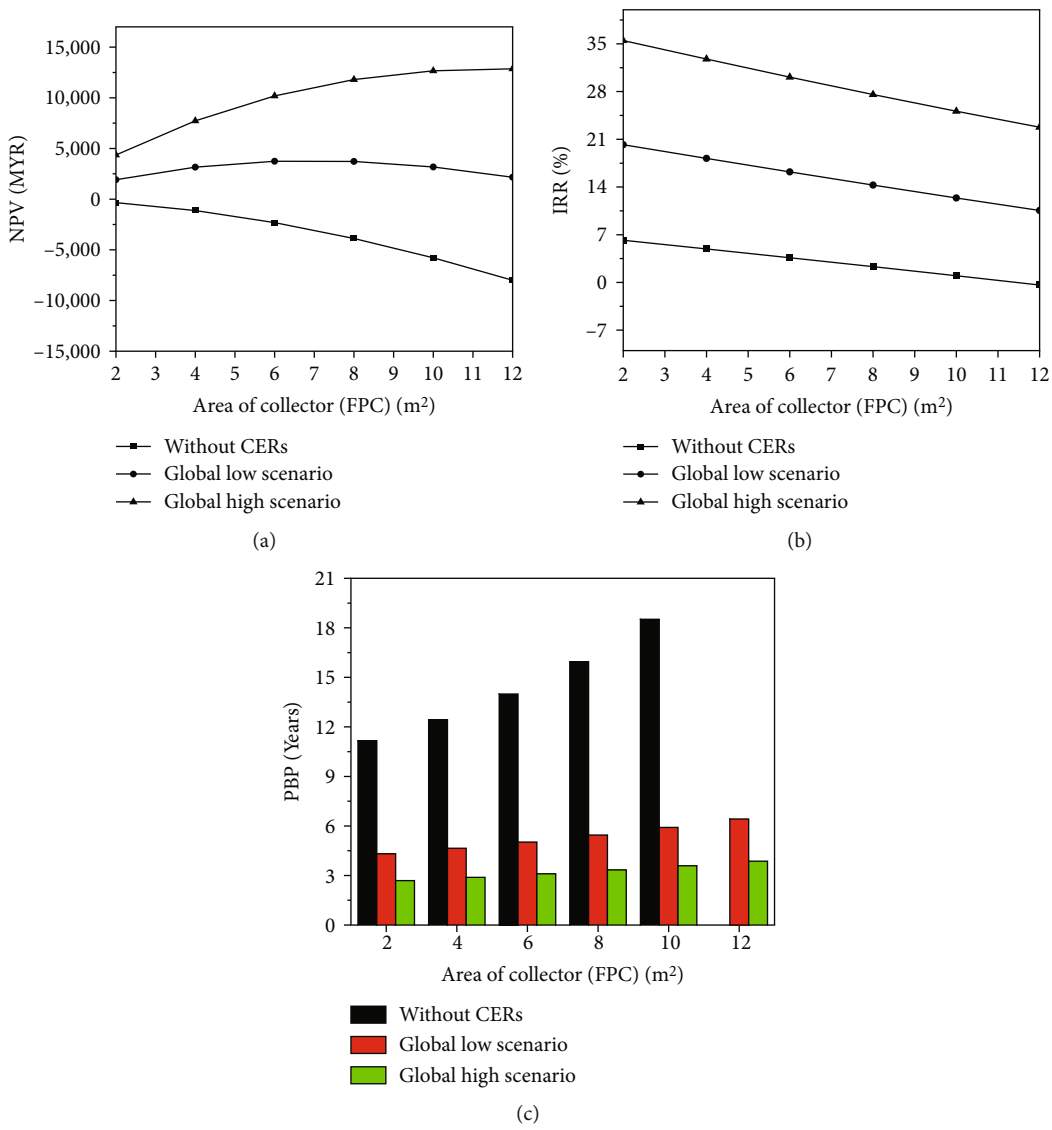

Figure 8: Variation in (a) NPV, (b) IRR, and (c) PBP as a function of collector area for isolated FPC system.

PBP is an investment appraisal technique which implies the amount of time taken by the investment to recover the initial investment, and it is calculated as a ratio of cash flow of *i*-th period and equivalent annual cash flow. In estimating the present value, a discount rate of 8% has been considered since the inflation rate in Malaysia is very low (3-4%) [71].

(1) Isolated PVT System. Figure 7(a) shows that for global low scenario (GLS), IRR increases to 20.53, 19.69, and 17.69% from only 3.75, 2.91, and 1.64% (without CER case) for 60, 70, and 80°C at 67.50, 64.54, and 61.67% solar energy penetration, respectively. Likewise, for the same process heat temperature and solar energy penetration, NPV increases to 5870.96, 6596.77, and 7080.64 RM from -2338.70, -3677.41, and -5274.19 RM (Figure 7(b)). On the other hand, under the same conditions, PBP reduces to 4.17, 4.42, and 4.65 years from 13.78, 15.32, and 17.09 years (without CERs), respectively (Figure 7(c)).

Similarly, for global high scenario (GHS), IRR is increased to 38.72, 37.04, and 34.30 from only 3.75, 2.91, and 1.64% (without CERs) for 60, 70, and 80°C at 67.50, 64.54, and 61.67% solar energy penetration, respectively. For the same process heat temperature and solar energy penetration, NPV increases to 14451.61, 17290.32, and 19758.06 RM from -2338.70, -3677.41, and -5274.19 RM (Figure 7(b)). Similarly, the payback period reduces to 2.52, 2.61, and 2.75 years from 13.78, 15.32, and 17.09 years (without CERs), respectively (Figure 7(c)).

(2) Isolated FPC System. Figure 8(a) shows that, for global low scenario (GLS), IRR is increased to 16.90, 15.58, and 13.98% from 4.07, 3.16, and 2.05% (without CERs) for 60, 70, and 80°C at 61.79, 59.29, and 56.59% solar energy penetration, respectively. Also, for the same process heat temperature and solar energy penetration, NPV increases to 3535.77, 3740.17, and 3674.80 RM from -1814.66, -2875.65, and

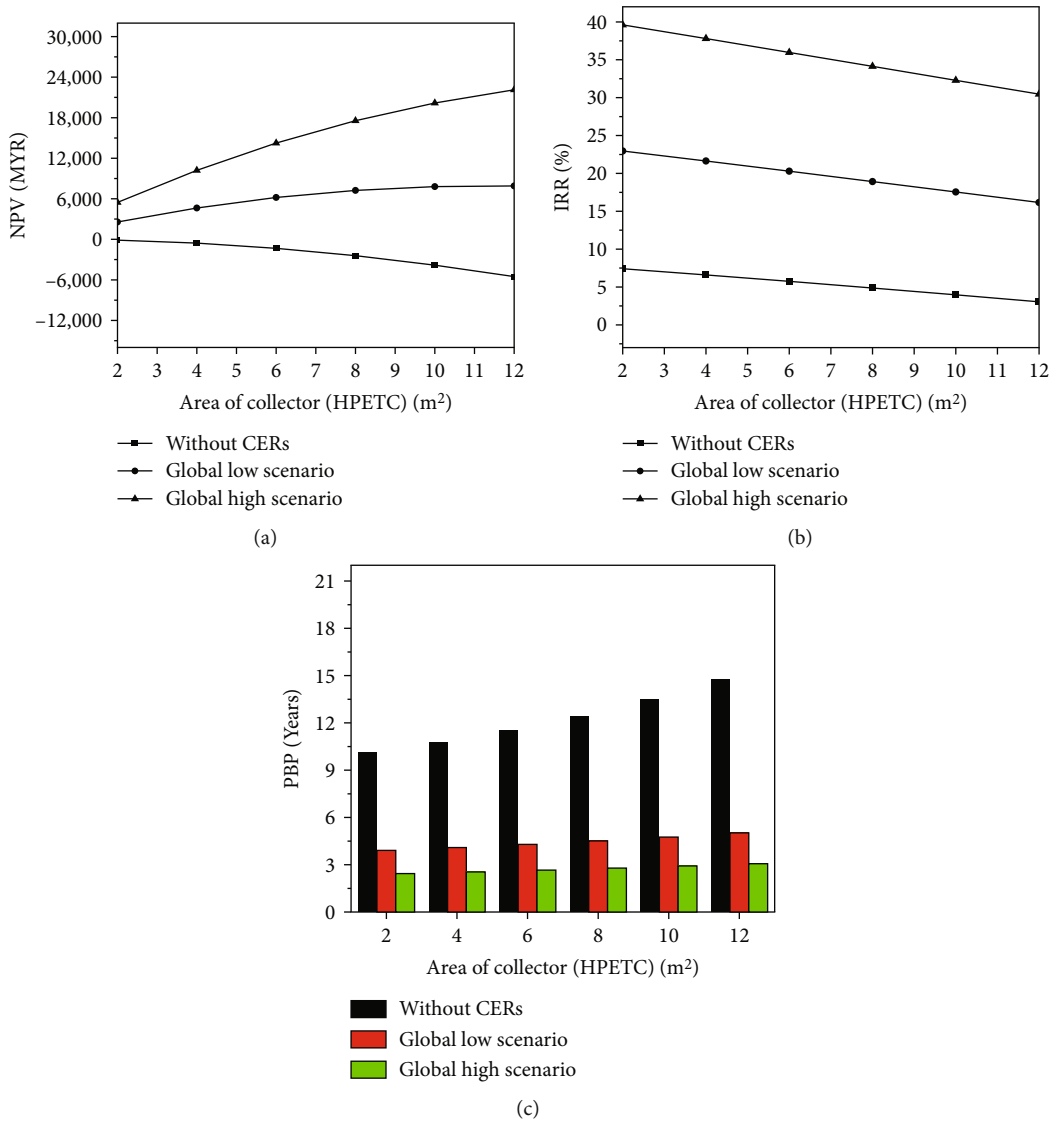

Figure 9: Variation in (a) NPV, (b) IRR, and (c) PBP as a function of collector area for isolated HPETC system.

-4170.67 RM (Figure 8(b)). In contrast, the payback period reduced to 4.92, 5.15, and 5.49 years from 13.41, 14.40, and 16.31 years (without CERs), respectively (Figure 8(c)).

For global high scenario (GHS), the internal rate of return is increased to 31.11, 29.23, and 27.40% from 4.07, 3.16, and 2.05% (without CERs) for 60, 70, and 80°C at 61.79, 59.29, and 56.59% solar energy penetration, respectively. Also, for the same process heat temperature and solar energy penetration, NPV increases to 9287.40, 10797.10, and 11885.55 RM from -1814.66, -2875.65, and -4170.67 RM (Figure 8(b)). Similarly, for the same process heat temperature and solar energy penetration, the payback period reduced to 3.06, 3.15, and 3.37 years from 13.41, 14.40, and 16.31 years (without CERs), respectively (Figure 8(c)).

(3) Isolated HPETC System. In the case of isolated HPETC system (Figures 9(a)–9(c)), for global low scenario (GLS), IRR is increased to 20.95%, 20.22%, and 19.14% from 6.25%, 5.64%, and 5.15% (without CERs) for 60, 70, and 80°C at 69.14%, 66.68%, and 64.95% solar energy penetration, respectively. For the same process heat temperature and solar energy penetration, NPV increases to 5381.81, 6324.92, and 7018.73 RM from -882.11, -1473.31, and -2177.21 RM, and the PBP reduced to 4.16, 4.33, and 4.45 years from 11.10, 11.62, and 12.23 years (without CERs), respectively.

Similarly, for global high scenario (GHS), IRR is increased to 36.86%, 35.75%, and 34.58% from 6.25, 5.64, and 5.15% (without CERs) for 60, 70, and 80°C at 69.14%, 66.68%, and 64.95% solar energy penetration, respectively. For the same process heat temperature and solar energy penetration, NPV increases to MYR 12082.16, MYR 14475.02, and MYR 16727.27 from MYR -882.11, MYR -1473.31, and MYR -2177.21, and the PBP reduced to 2.63, 2.71, and 2.79 years from 11.10, 11.62, and 12.23 years (without CERs), respectively.

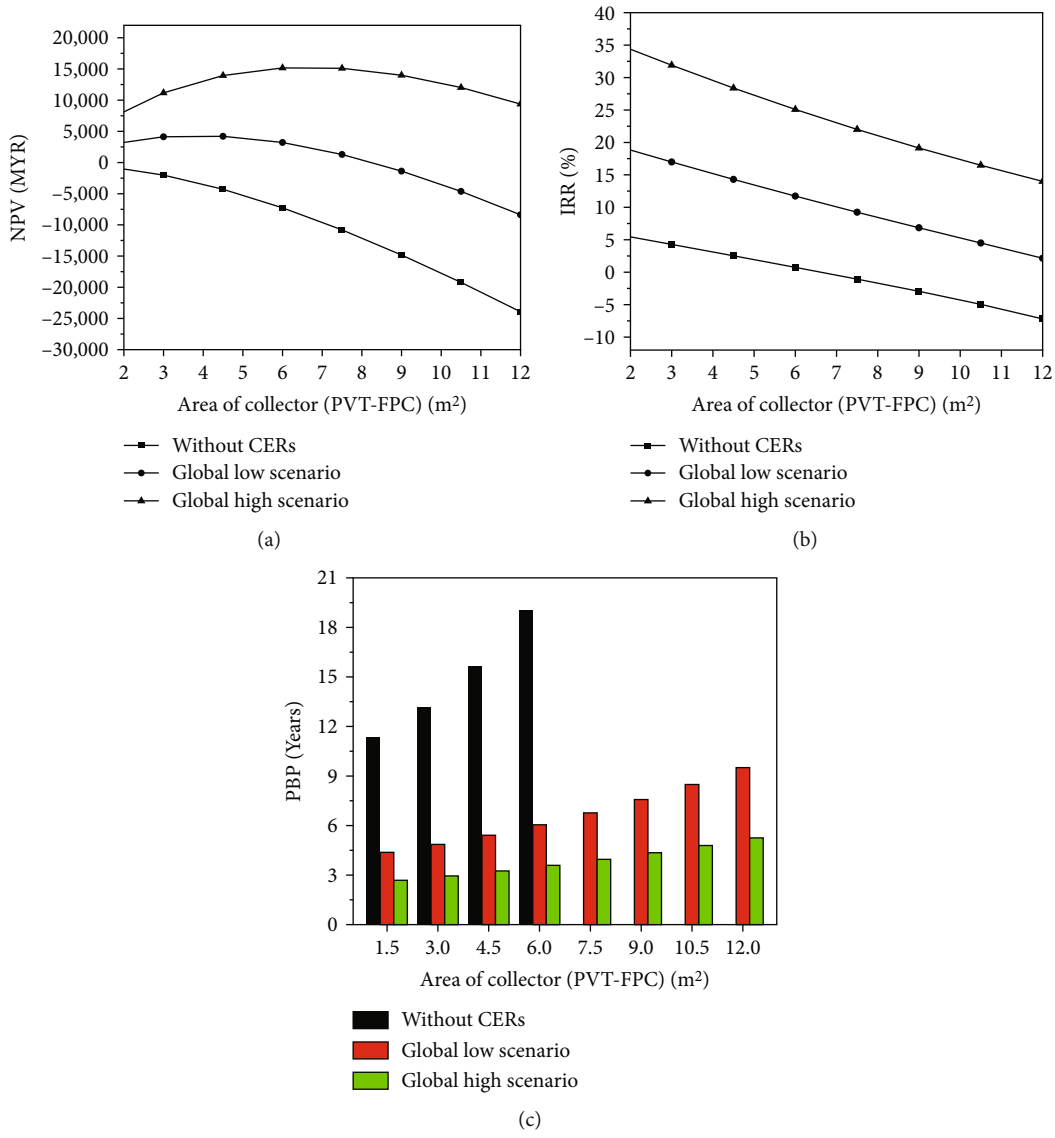

Figure 10: Variation in (a) NPV, (b) IRR, and (c) PBP as a function of collector area for cascaded PVT-FPC system.

(4) Cascaded PVT-FPC System. In the case of cascaded PVT-FPC system (Figures 10(a)–10(c)), for global low scenario (GLS), IRR is increased to 15.82%, 14.15%, and 12.30% from 3.52%, 2.33%, and 1.12% (without CERs) for 60, 70, and 80°C at 65.01, 61.58, and 58.26% solar energy penetration, respectively. For the same process heat temperature and solar energy penetration, NPV increases to MYR 4127.85, MYR 4036.36, and MYR 3411.14 from MYR -3069.79, MYR -4579.47, and MYR -6653.37, and the PBP reduced to 5.02, 5.43, and 5.91 years from 14.20, 15.90, and 18.05 years (without CERs), respectively.

Similarly, for the global high scenario (GHS), IRR is increased to 30.36%, 28.04%, and 25.80% from 3.52%, 2.33%, and 1.12% (without CERs) for 60, 70, and 80°C at 65.01%, 61.58%, and 58.26% solar energy penetration, respectively. For the same process heat temperature and solar energy penetration, NPV increases to MYR 12347.21, MYR 14024.63, and MYR 14909.09 from MYR -3069.79, MYR -4579.47, and MYR -6653.37, and the PBP reduced to 3.08, 3.25, and 3.49 years from 14.20, 15.90, and 18.05 years (without CERs), respectively.

(5) Cascaded PVT-HPETC System. In the case of cascaded PVT-HPETC system (Figures 11(a)–11(c)), for the global low scenario (GLS), IRR is increased to 20.25%, 18.95%, and 17.50% from 5.12%, 4.34%, and 3.35% (without CERs) for 60, 70, and 80°C at 78.50%, 75.71%, and 73.10% solar energy penetration, respectively. For the same process heat temperature and solar energy penetration, NPV increases to MYR 7537.25, MYR 8650.83, and MYR 9102.05 from MYR -2157.77, MYR -3518.47, and MYR -4930.20, and the PBP reduced to 4.30, 4.50, and 4.86 years from 12.22, 13.25, and 14.30 years (without CERs), respectively.

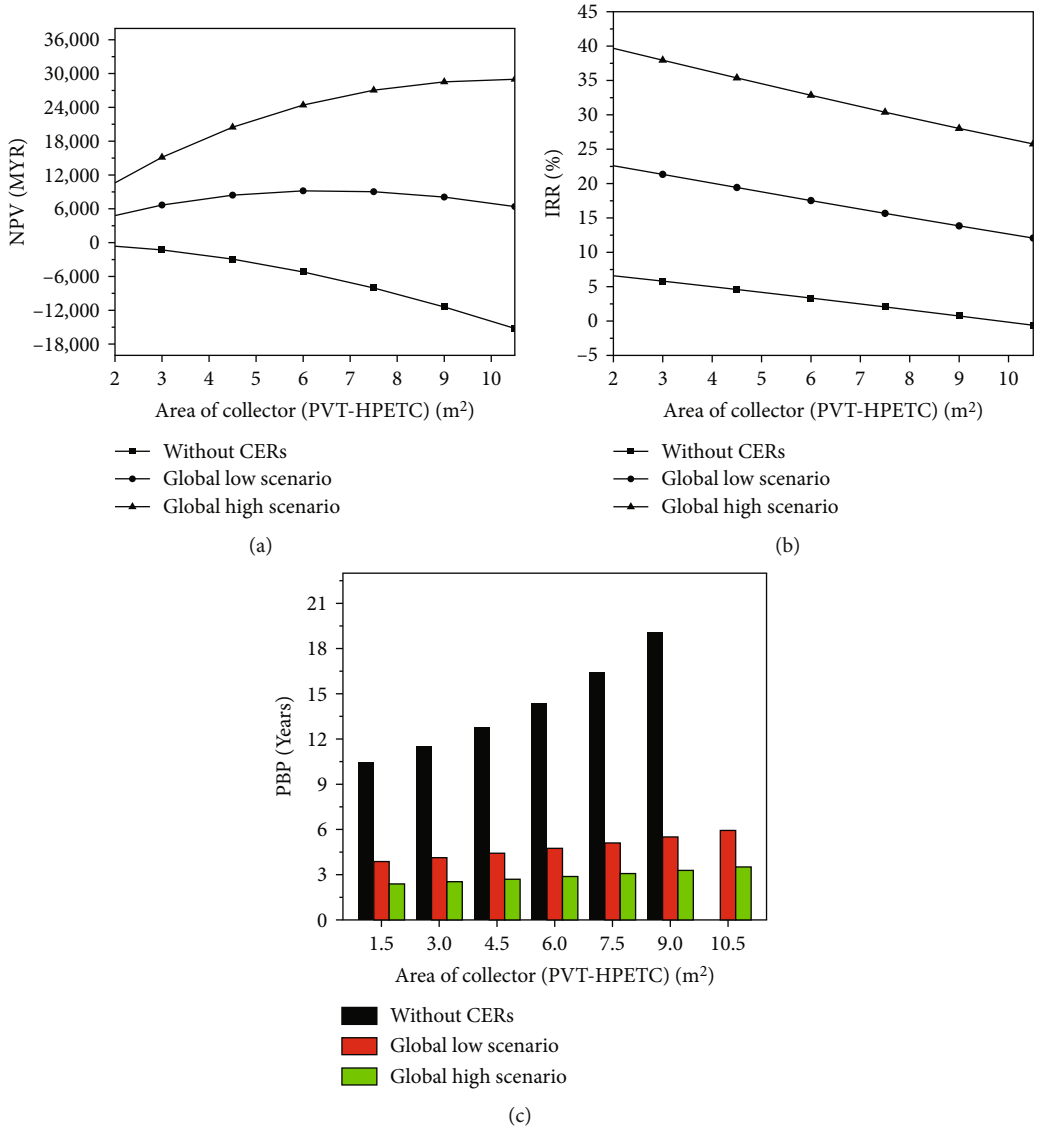

Figure 11: Variation in (a) NPV, (b) IRR, and (c) PBP as a function of collector area for cascaded PVT-HPETC system.

Similarly, for the global high scenario (GHS), IRR is increased to 36.55%, 34.80%, and 33.15% from 5.12%, 4.34%, and 3.35% (without CERs) for 60, 70, and 80°C at 78.50%, 75.71%, and 73.10% solar energy penetration, respectively. For the same process heat temperature and solar energy penetration, NPV increases to MYR 18099.67, MYR 21350.55, and MYR 23814.10 from MYR -2157.77, MYR -3518.47, and MYR -4930.20, and the PBP reduced to 2.63, 2.77, and 2.89 years from 12.22, 13.25, and 14.30 years (without CERs), respectively.

Thus, it can be concluded that the involvement of CERs in both scenarios plays an important role in attracting the use of these technologies in a broader perspective. Internal rate return (IRR) is a measure of the project profitability. If the IRR of the project is higher and more than the minimum attractive rate of return (MARR) (usually >10%), then it is defined as a profitable project [55]. It may be also concluded from the above discussion that for the same area of collector required, the solar energy penetration increased significantly in the case of isolated HPETC and cascaded PVT-HPETC systems as compared to other isolated and cascaded systems.

3.3.2. Levelized Cost of Heat (LCOH) Analysis. In order to adequately compare isolated and cascaded systems, a standard metric, LCOH, has been employed that combines two disparate energy flows (i.e., heat and electricity) into one bottom-line metric. The proposed LCOH model is applied to both isolated and cascaded systems, and results are illustrated in Figures 12(a) and 12(b). It can be seen from the figure that the cascaded systems offer a reduced LCOH in comparison to isolated installations at the same solar energy penetration, as much of the cost in the hybrid system is shared between the electric and thermal subsystems. Due to the higher collector efficiency of the cascaded system, the total collector area can be reduced, and solar energy penetration share can be increased.

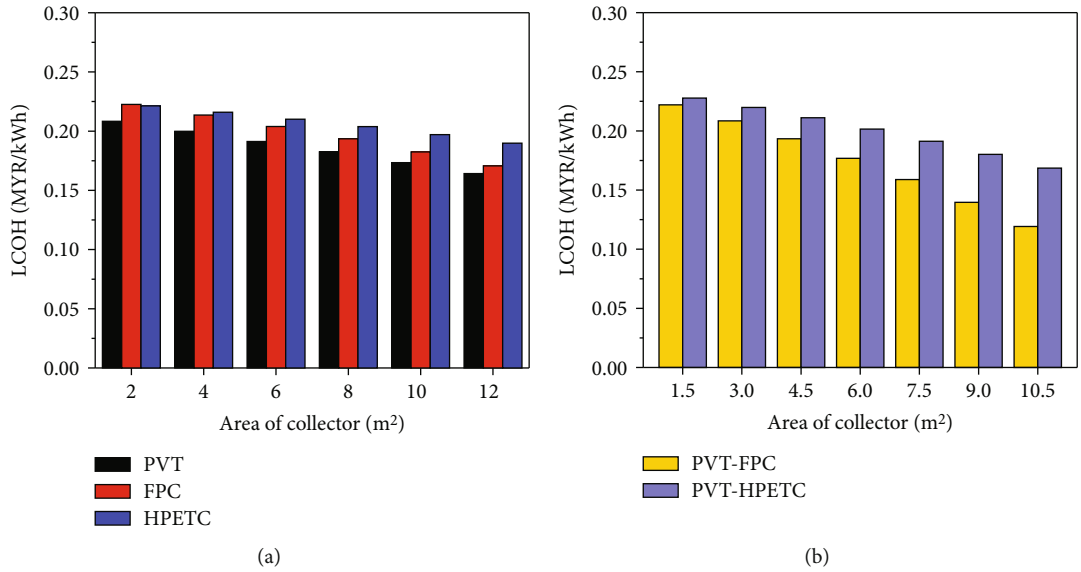

Figure 12: LCOH as a function of collector area for (a) isolated systems and (b) cascaded systems.

In the case of isolated systems (Figure 12(a)), the LCOH of the PVT system is lower than both FPC and PVT due to simultaneous heat and electricity production; however, the solar energy penetration is higher for isolated HPETC than the other two systems. For the PVT system, LCOH at process heat temperature (60, 70, and 80°C) and solar energy penetration (67.50%, 64.54%, and 61.67%) is MYR 0.193, MYR 0.184, and MYR 0.176 per kWh, respectively. In the case of the FPC system, LCOH at process heat temperature (60, 70, and 80°C) and solar energy penetration (61.79%, 59.29%, and 56.59%) is MYR 0.207, MYR 0.199, and MYR 0.192 per kWh, respectively. And for the HPETC system, LCOH at process heat temperature (60, 70, and 80°C) and solar energy penetration (69.14%, 66.68%, and 64.95%) is MYR 0.211, MYR 0.208, and MYR 0.204 per kWh, respectively.

In the case of cascaded systems (Figure 12(b)), the LCOH of the PVT-FPC system is lower than PVT-HPETC due to the low capital cost; however, the solar energy penetration is higher in the case of PVT-HPETC than PVT-FPC system for the same collector area. For the PVT-FPC system, LCOH at process heat temperature (60, 70, and 80°C) and solar energy penetration (65.01%, 61.58%, and 58.26%) is MYR 0.203, MYR 0.193, and MYR 0.181 per kWh, respectively. In comparison, LCOH for PVT-HPETC at process heat temperature (60, 70, and 80°C) and solar energy penetration (78.50%, 75.71%, and 73.10%) is MYR 0.214, MYR 0.208, and MYR 0.201 per kWh, respectively.

However, it is worth to note that LCOH for all the cases is less than the existing cost of heat generation which proves that these systems are economically feasible. Overall, the PVT-HPETC system performs better and gives the higher solar energy penetration at low collector areas.

From the discussions in the preceding sections, it is quite apparent that none of the systems are economically feasible without CER for every process temperature (60, 70, or 80°C), which is evident from the negative values of NPV, very low IRR, and high PBP. On the other hand, the introduction of CERs (be it with GLS or GHS) brings about significant changes in NPV, IRR, and PBP values.

4. Conclusions

A novel solar-assisted process heating (SAPH) system has been designed to realize low to medium industrial process heat demand at minimum fossil fuel usage. A dynamic simulation model has been built in TRNSYS to predict the optimum configuration and performance of this system at different flow rates of the heat transfer fluid. The model has been authenticated through prototype implementation and outdoor experimentation. Outlet water temperature, solar energy penetration, and annual energy generated increase with an increase in collector area. Therefore, collector area optimization is important to select an optimum collector area that can fulfil our selected process heat temperatures (60, 70, and 80°C).

The major inferences from the thermoeconomic analysis are summarized as follows:

(i) Maximum outlet temperatures of water achieved with PVT-HPETC and PVT-FPC systems are 71.5 and 66°C, while that with isolated HPETC and FPC system are 60.5 and 56°C

(ii) Maximum energy (thermal) efficiency of PVT-HPETC and PVT-FPC system are 81% and 77%, respectively

(iii) PVT-HPETC and PVT-FPC systems achieved the maximum exergy efficiency of 13.22% and 12.72%, respectively

(iv) Performance mapping ascertains that SAPH performs better at an optimum mass flow rate of 1.0 LPM

(v) The optimized collector area for different systems are

(a) In the case of the PVT system, 5.43, 7.26, and 9.25 m^2 for 60, 70, and 80°C process temperatures, respectively

(b) In the case of the FPC system, 5.26, 6.74, and 8.26 m^2 for 60, 70, and 80°C process temperatures, respectively

(c) In the case of the HPETC system, 4.93, 6.21, and 7.55 m^2 for 60, 70, and 80°C process temperatures, respectively

(d) In the case of the PVT-FPC system, 3.08, 4.17, and 5.32 m^2 for 60, 70, and 80°C process temperatures, respectively

(e) In the case of the PVT-HPETC system, 3.85, 4.98, and 6.10 m^2 for 60, 70, and 80°C process temperatures, respectively

(vi) In the case of the HPETC system and GLS, the IRR and PBP obtained are 21.64, 20.29, and 18.92% and 4.09, 4.29, and 4.51 years for 60, 70, and 80°C, respectively

(vii) In the case of the HPETC system and GHS, the IRR and PBP obtained are 37.81%, 35.97%, and 34.13% and 2.54, 2.66, and 2.78 years for 60, 70, and 80°C, respectively

(viii) In the case of the PVT-HPETC system and GLS, the IRR and PBP obtained are 22.28%, 21.33%, and 20.38% and 4.00, 4.13, and 4.28 years for 60, 70, and 80°C, respectively

(ix) In the case of the PVT-HPETC system and GHS, the IRR and PBP obtained are 39.24%, 37.95%, and 36.66% and 2.46, 2.54, and 2.62 years for 60, 70, and 80°C, respectively

(x) LCOH for HPETC and PVT-HPETC at process heat temperatures of 60, 70, and 80°C are 0.224, 0.219, and 0.215 MYR/kWh, and 0.216, 0.210, and 0.204 MYR/kWh, respectively. It is worth to note that LCOH is less than the existing cost of heat generation which proves that these systems are economically feasible

Nomenclature

A: Collector area (m^2)
c_p: Constant pressure specific heat (J/Kg K)
CF: Cash flow
D: Diameter
dr: Discount rate
$\dot{E}$: Energy
ES: Electricity savings
I: Solar irradiance (W/m^2)
IP: Improvement potential
I_{max}: Maximum current
I_{sc}: Short-circuit current
m: Mass flow rate of fluid (kg/s)
N: Number
n_1: Day of the year
OM: Operation and maintenance cost
PV: Present value
Q_1: Latitude of the experimental location
$\dot{S}$: Entropy
T: Temperature (°C or K)
t: Thickness (m)
V_{max}: Maximum voltage
V_{oc}: Open-circuit voltage
W: Heat (W).

Greek letters

a_0: Intercept efficiency
a_1: Efficiency slope
a_2: Efficiency curvature
δ: Angle of inclination
α: Coefficient of absorptance
β: Orientation angle towards the equator
n_1: Specific day number of the year
τ: Coefficient of transmittance
η: Efficiency.

Indices

a: Ambient
c: Collector
CS: Cascaded system
dest: Destruction
el: Electrical
exp: Experimental
g: Gain
gc: Glazing cover
hp: Heat pipe
i: In/inner/inlet
o: Out/outer/outlet
ov: Overall
p: Aperture
s: Sun
sim: Simulated
th: Thermal
x: Exergy.

Data Availability

Data will be made available on request.

Additional Points

Highlights. (i) Thermoeconomic analysis of PVT-FPC and PVT-HPETC systems. (ii) TRNSYS models of the cascaded systems are validated by outdoor experimentations. (iii) Maximum energy efficiency of PVT-HPETC and PVT-FPC systems is 81% and 77%, respectively. (iv) Maximum exergy efficiency of PVT-HPETC and PVT-FPC systems is 13.22

and 12.72%, respectively. (v) LCOH is less than the existing cost of heat generation

Disclosure

The findings herein reflect the work and are solely the responsibility of the authors. A preprint of this work has previously been published [72]. This current version represents an updated and peer-reviewed version of the manuscript. The authors would like to acknowledge that an earlier version of this manuscript has been presented as a preprint in the Social Science Research Network (SSRN) at the following link: (https://papers.ssrn.com/sol3/papers.cfm?abstract_id=4048138).

Conflicts of Interest

The authors declare that they have no known competing financial interests or personal relationships that could have appeared to influence the work reported in this paper.

Authors' Contributions

Laveet Kumar was responsible for conceptualization, data curation, formal analysis, investigation, methodology, software, validation, visualization, and writing the original draft. M. Hasanuzzaman was responsible for conceptualization, formal analysis, writing, reviewing, editing, supervision, and project administration. N.A. Rahim was responsible for writing, reviewing, editing, supervision, and project administration. Ahmad K. Sleiti was responsible for writing, reviewing, editing, supervision, and project administration.

Acknowledgments

The authors acknowledge the financial support of Open Access from the Qatar National Library. This publication was also supported by the Post-Doc Research Program, Qatar University (QUPD-CENG-23-24-537). We would like to express our gratitude to SSRN for providing a platform for the dissemination of our initial findings.

References

[1] M. Hosenuzzaman, N. A. Rahim, J. Selvaraj, M. Hasanuzzaman, A. B. M. A. Malek, and A. Nahar, "Global prospects, progress, policies, and environmental impact of solar photovoltaic power generation," *Renewable and Sustainable Energy Reviews*, vol. 41, pp. 284–297, 2015.

[2] R. Kumar and M. A. Rosen, "A critical review of photovoltaic–thermal solar collectors for air heating," *Applied Energy*, vol. 88, no. 11, pp. 3603–3614, 2011.

[3] M. Hasanuzzaman, N. A. Rahim, M. Hosenuzzaman, R. Saidur, I. M. Mahbubul, and M. M. Rashid, "Energy savings in the combustion-based process heating in industrial sector," *Renewable and Sustainable Energy Reviews*, vol. 16, no. 7, pp. 4527–4536, 2012.

[4] E. A. Abdelaziz, R. Saidur, and S. Mekhilef, "A review on energy saving strategies in industrial sector," *Renewable and Sustainable Energy Reviews*, vol. 15, no. 1, pp. 150–168, 2011.

[5] L. Kumar, M. Hasanuzzaman, and N. Rahim, "Global advancement of solar thermal energy technologies for industrial process heat and its future prospects: a review," *Energy Conversion Management*, vol. 195, pp. 885–908, 2019.

[6] Intergovernmental Panel on Climate Chan, *Synthesis Report. Contribution of working groups I II III to the Fifth Assessment Report*, Intergovernmental Panel on Climate Change (IPCC), 2014, 151 (10.1017).

[7] D. Einstein, E. Worrell, and M. Khrushch, *Steam systems in industry: energy use and energy efficiency improvement potentials*, Lawrence Berkeley National Lab (LBNL), Berkeley, CA (United States), 2001.

[8] S. Kalogirou, "The potential of solar industrial process heat applications," *Applied Energy*, vol. 76, no. 4, pp. 337–361, 2003.

[9] International Energy Agency (IEA), *CO2 Emissions from Fuel Combustion 2017*, Organisation for Economic Co-operation and Development (OECD), 2017.

[10] R. J. Fuller, "Solar industrial process heating in Australia–past and current status," *Renewable Energy*, vol. 36, no. 1, pp. 216–221, 2011.

[11] T. Sokhansefat, A. Kasaeian, K. Rahmani, A. H. Heidari, F. Aghakhani, and O. Mahian, "Thermoeconomic and environmental analysis of solar flat plate and evacuated tube collectors in cold climatic conditions," *Renewable Energy*, vol. 115, pp. 501–508, 2018.

[12] A. Nahar, M. Hasanuzzaman, N. A. Rahim, and S. Parvin, "Numerical investigation on the effect of different parameters in enhancing heat transfer performance of photovoltaic thermal systems," *Renewable Energy*, vol. 132, pp. 284–295, 2019.

[13] ESTTP, *Cooling for a Sustainable Energy Future in Europe (Revised)*, European Solar Thermal Technology Platform (ESTTP), 2009.

[14] H. Fayaz, N. A. Rahim, M. Hasanuzzaman, A. Rivai, and R. Nasrin, "Numerical and outdoor real time experimental investigation of performance of PCM based PVT system," *Solar Energy*, vol. 179, pp. 135–150, 2019.

[15] T. Ma, H. Yang, and L. Lu, "Solar photovoltaic system modeling and performance prediction," *Renewable and Sustainable Energy Reviews*, vol. 36, pp. 304–315, 2014.

[16] W. Weiss and F. Mauthner, *Solar Heat Worldwide*, IEA Solar Heating and Cooling Programme, 2010.

[17] P. D. Myers and D. Y. Goswami, "Thermal energy storage using chloride salts and their eutectics," *Applied Thermal Engineering*, vol. 109, pp. 889–900, 2016.

[18] Y. Bhusal, A. Hassanzadeh, L. Jiang, and R. Winston, "Technical and economic analysis of a novel low-cost concentrated medium-temperature solar collector," *Renewable Energy*, vol. 146, pp. 968–985, 2020.

[19] T. Ma, M. Li, and A. Kazemian, "Photovoltaic thermal module and solar thermal collector connected in series to produce electricity and high-grade heat simultaneously," *Applied Energy*, vol. 261, p. 114380, 2020.

[20] M. Ghazouani, M. Bouya, and M. Benaissa, "Thermo-economic and exergy analysis and optimization of small PTC collectors for solar heat integration in industrial processes," *Renewable Energy*, vol. 152, pp. 984–998, 2020.

[21] A. Kazemian, A. Taheri, A. Sardarabadi, T. Ma, M. Passandideh-Fard, and J. Peng, "Energy, exergy and environmental analysis of glazed and unglazed PVT system integrated with phase change material: an experimental approach," *Solar Energy*, vol. 201, pp. 178–189, 2020.

[22] A. Kazemian, M. Hosseinzadeh, M. Sardarabadi, and M. Passandideh-Fard, "Effect of glass cover and working fluid on the performance of photovoltaic thermal (PVT) system: an experimental study," *Solar Energy*, vol. 173, pp. 1002–1010, 2018.

[23] A. Kazemian, M. Hosseinzadeh, M. Sardarabadi, and M. Passandideh-Fard, "Experimental study of using both ethylene glycol and phase change material as coolant in photovoltaic thermal systems (PVT) from energy, exergy and entropy generation viewpoints," *Energy*, vol. 162, pp. 210–223, 2018.

[24] T. T. Chow, G. Pei, K. F. Fong, Z. Lin, A. L. S. Chan, and J. Ji, "Energy and exergy analysis of photovoltaic–thermal collector with and without glass cover," *Applied Energy*, vol. 86, no. 3, pp. 310–316, 2009.

[25] J. F. Chen, L. Zhang, and Y. J. Dai, "Performance analysis and multi-objective optimization of a hybrid photovoltaic/thermal collector for domestic hot water application," *Energy*, vol. 143, pp. 500–516, 2018.

[26] I. Guarracino, J. Freeman, A. Ramos, S. A. Kalogirou, N. J. Ekins-Daukes, and C. N. Markides, "Systematic testing of hybrid PV-thermal (PVT) solar collectors in steady-state and dynamic outdoor conditions," *Applied Energy*, vol. 240, pp. 1014–1030, 2019.

[27] A. Asanakham and T. Deethayat, "Performance analysis of PV/T modules with and without glass cover and effect of mass flow rate on electricity and hot water generation," *Energy Reports*, vol. 6, pp. 558–564, 2020.

[28] A. N. Al-Shamani, K. Sopian, S. Mat, H. A. Hasan, A. M. Abed, and M. H. Ruslan, "Experimental studies of rectangular tube absorber photovoltaic thermal collector with various types of nanofluids under the tropical climate conditions," *Energy Conversion and Management*, vol. 124, pp. 528–542, 2016.

[29] M. Herrando, A. Ramos, I. Zabalza, and C. N. Markides, "A comprehensive assessment of alternative absorber-exchanger designs for hybrid PVT-water collectors," *Applied Energy*, vol. 235, pp. 1583–1602, 2019.

[30] O. Rejeb, L. Gaillard, S. Giroux-Julien et al., "Novel solar PV/thermal collector design for the enhancement of thermal and electrical performances," *Renewable Energy*, vol. 146, pp. 610–627, 2020.

[31] F. Chen, M. Hu, A. Badiei et al., "Experimental and numerical investigation of a novel photovoltaic/thermal system using micro-channel flat loop heat pipe (PV/T-MCFLHP)," *International Journal of Low-Carbon Technologies*, vol. 15, no. 4, pp. 513–527, 2020.

[32] M. S. Hossain, A. K. Pandey, J. Selvaraj, N. Abd Rahim, A. Rivai, and V. V. Tyagi, "Thermal performance analysis of parallel serpentine flow based photovoltaic/thermal (PV/T) system under composite climate of Malaysia," *Applied Thermal Engineering*, vol. 153, pp. 861–871, 2019.

[33] M. S. Hossain, A. K. Pandey, J. Selvaraj, N. A. Rahim, M. M. Islam, and V. V. Tyagi, "Two side serpentine flow based photovoltaic-thermal-phase change materials (PVT-PCM) system: energy, exergy and economic analysis," *Renewable Energy*, vol. 136, pp. 1320–1336, 2019.

[34] Y. Tong, H. Lee, W. Kang, and H. Cho, "Energy and exergy comparison of a flat-plate solar collector using water, Al_2O_3 nanofluid, and CuO nanofluid," *Applied Thermal Engineering*, vol. 159, article 113959, 2019.

[35] Z. Said, R. Saidur, M. A. Sabiha, A. Hepbasli, and N. A. Rahim, "Energy and exergy efficiency of a flat plate solar collector using pH treated Al2O3 nanofluid," *Journal of Cleaner Production*, vol. 112, pp. 3915–3926, 2016.

[36] Z. Said, R. Saidur, and N. A. Rahim, "Energy and exergy analysis of a flat plate solar collector using different sizes of aluminium oxide based nanofluid," *Journal of Cleaner Production*, vol. 133, pp. 518–530, 2016.

[37] H. Gunerhan and A. Hepbasli, "Exergetic modeling and performance evaluation of solar water heating systems for building applications," *Energy and Buildings*, vol. 39, no. 5, pp. 509–516, 2007.

[38] D. G. Gunjo, P. Mahanta, and P. S. Robi, "Exergy and energy analysis of a novel type solar collector under steady state condition: experimental and CFD analysis," *Renewable Energy*, vol. 114, pp. 655–669, 2017.

[39] S. Farahat, F. Sarhaddi, and H. Ajam, "Exergetic optimization of flat plate solar collectors," *Renewable Energy*, vol. 34, no. 4, pp. 1169–1174, 2009.

[40] S. A. Kalogirou, S. Karellas, K. Braimakis, C. Stanciu, and V. Badescu, "Exergy analysis of solar thermal collectors and processes," *Progress in Energy and Combustion Science*, vol. 56, pp. 106–137, 2016.

[41] F. Jafarkazemi and E. Ahmadifard, "Energetic and exergetic evaluation of flat plate solar collectors," *Renewable Energy*, vol. 56, pp. 55–63, 2013.

[42] Z. Ge, H. Wang, H. Wang, S. Zhang, and X. Guan, "Exergy analysis of flat plate solar collectors," *Entropy*, vol. 16, no. 5, pp. 2549–2567, 2014.

[43] A. Başçetinçelik, H. H. Öztürk, H. Ö. Paksoy, and Y. Demirel, "Energetic and exergetic efficiency of latent heat storage system for greenhouse heating," *Renewable Energy*, vol. 16, no. 1-4, pp. 691–694, 1999.

[44] A. Koca, H. F. Oztop, T. Koyun, and Y. Varol, "Energy and exergy analysis of a latent heat storage system with phase change material for a solar collector," *Renewable Energy*, vol. 33, no. 4, pp. 567–574, 2008.

[45] M. Li, D. Zhong, T. Ma, A. Kazemian, and W. Gu, "Photovoltaic thermal module and solar thermal collector connected in series: energy and exergy analysis," *Energy Conversion and Management*, vol. 206, article 112479, 2020.

[46] M. Malaysia, *MET Malaysia annual report 2019*, R. A. Rahman, Ed., Malaysian Meteorological Department, Malaysia, 2020.

[47] P. I. Cooper, "The absorption of radiation in solar stills," *Solar Energy*, vol. 12, no. 3, pp. 333–346, 1969.

[48] R. Daghigh and A. Shafieian, "Theoretical and experimental analysis of thermal performance of a solar water heating system with evacuated tube heat pipe collector," *Applied Thermal Engineering*, vol. 103, pp. 1219–1227, 2016.

[49] L. Kumar, M. Hasanuzzaman, N. A. Rahim, and M. M. Islam, "Modeling, simulation and outdoor experimental performance analysis of a solar-assisted process heating system for industrial process heat," *Renewable Energy*, vol. 164, pp. 656–673, 2021.

[50] M. Sardarabadi, M. Hosseinzadeh, A. Kazemian, and M. Passandideh-Fard, "Experimental investigation of the effects of using metal-oxides/water nanofluids on a photovoltaic thermal system (PVT) from energy and exergy viewpoints," *Energy*, vol. 138, pp. 682–695, 2017.

[51] S. R. Park, A. K. Pandey, V. V. Tyagi, and S. K. Tyagi, "Energy and exergy analysis of typical renewable energy systems,"

Renewable and Sustainable Energy Reviews, vol. 30, pp. 105–123, 2014.

[52] A. Fudholi, M. Zohri, G. L. Jin et al., "Energy and exergy analyses of photovoltaic thermal collector with ∇-groove," *Solar Energy*, vol. 159, pp. 742–750, 2018.

[53] M. Sardarabadi, M. Passandideh-Fard, and S. Zeinali Heris, "Experimental investigation of the effects of silica/water nanofluid on PV/T (photovoltaic thermal units)," *Energy*, vol. 66, pp. 264–272, 2014.

[54] L. Kumar, M. A. A. Mamun, and M. Hasanuzzaman, *Chapter 7- energy economics, in Energy for Sustainable Development*, M. D. Hasanuzzaman and N. A. Rahim, Eds., Academic Press, 2020.

[55] A. M. Vale, D. G. Felix, M. Z. Fortes, B. S. M. C. Borba, B. H. Dias, and B. S. Santelli, "Analysis of the economic viability of a photovoltaic generation project applied to the Brazilian housing program "Minha Casa Minha Vida"," *Energy Policy*, vol. 108, pp. 292–298, 2017.

[56] B. C. Riggs, R. Biedenharn, C. Dougher et al., "Techno-economic analysis of hybrid PV/T systems for process heat using electricity to subsidize the cost of heat," *Applied Energy*, vol. 208, pp. 1370–1378, 2017.

[57] A. H. A. Al-Waeli, M. T. Chaichan, K. Sopian, H. A. Kazem, H. B. Mahood, and A. A. Khadom, "Modeling and experimental validation of a PVT system using nanofluid coolant and nano-PCM," *Solar Energy*, vol. 177, pp. 178–191, 2019.

[58] A. H. A. Al-Waeli, K. Sopian, M. T. Chaichan et al., "Evaluation of the nanofluid and nano-PCM based photovoltaic thermal (PVT) system: an experimental study," *Energy Conversion and Management*, vol. 151, pp. 693–708, 2017.

[59] H. Fayaz, N. A. Rahim, M. Hasanuzzaman, R. Nasrin, and A. Rivai, "Numerical and experimental investigation of the effect of operating conditions on performance of PVT and PVT-PCM," *Renewable Energy*, vol. 143, pp. 827–841, 2019.

[60] A. Ibrahim, A. Fudholi, K. Sopian, M. Y. Othman, and M. H. Ruslan, "Efficiencies and improvement potential of building integrated photovoltaic thermal (BIPVT) system," *Energy Conversion and Management*, vol. 77, pp. 527–534, 2014.

[61] A. Nahar, M. Hasanuzzaman, and N. A. Rahim, "Numerical and experimental investigation on the performance of a photovoltaic thermal collector with parallel plate flow channel under different operating conditions in Malaysia," *Solar Energy*, vol. 144, pp. 517–528, 2017.

[62] S. K. Verma, A. K. Tiwari, and D. S. Chauhan, "Performance augmentation in flat plate solar collector using MgO/water nanofluid," *Energy Conversion and Management*, vol. 124, pp. 607–617, 2016.

[63] O. A. Hussein, K. Habib, A. S. Muhsan, R. Saidur, O. A. Alawi, and T. K. Ibrahim, "Thermal performance enhancement of a flat plate solar collector using hybrid nanofluid," *Solar Energy*, vol. 204, pp. 208–222, 2020.

[64] M. A. Sabiha, R. Saidur, S. Hassani, Z. Said, and S. Mekhilef, "Energy performance of an evacuated tube solar collector using single walled carbon nanotubes nanofluids," *Energy Conversion and Management*, vol. 105, pp. 1377–1388, 2015.

[65] M. A. Sharafeldin and G. Gróf, "Efficiency of evacuated tube solar collector using WO3/water nanofluid," *Renewable Energy*, vol. 134, pp. 453–460, 2019.

[66] L. M. Ayompe, A. Duffy, M. Mc Keever, M. Conlon, and S. J. McCormack, "Comparative field performance study of flat plate and heat pipe evacuated tube collectors (ETCs) for domestic water heating systems in a temperate climate," *Energy*, vol. 36, no. 5, pp. 3370–3378, 2011.

[67] M. Hosseinzadeh, M. Sardarabadi, and M. Passandideh-Fard, "Energy and exergy analysis of nanofluid based photovoltaic thermal system integrated with phase change material," *Energy*, vol. 147, pp. 636–647, 2018.

[68] UNFCCC, "Emission Trading GHGs," 2021, https://unfccc.int/process/the-kyoto-protocol/mechanisms/emissions-trading.

[69] LHDN, 2021, http://www.hasil.gov.my/.

[70] WBG, *State and Trends of Carbon Pricing*, World Bank Group (WBG), Washington, DC, 2019.

[71] A. B. M. Abdul Malek, M. Hasanuzzaman, N. A. Rahim, and Y. A. Al-Turki, "Energy, economic, and environmental analysis of 10-MW biomass gasification based power generation in Malaysia," *Energy & Environment*, vol. 32, no. 2, pp. 295–337, 2021.

[72] L. Kumar, M. Hasanuzzaman, and P. J. N. Abd Rahim, "Thermo-economic analysis of a solar-assisted industrial process heating system," *Nasrudin, Thermo-Economic Analysis of a Solar-Assisted Industrial Process Heating System*, https://papers.ssrn.com/sol3/papers.cfm?abstract_id=4048138.